Int J Adv Manuf Technol (2015) 78:465–480
DOI 10.1007/s00170-014-6600-2

ORIGINAL ARTICLE

Numerical analysis of the interaction between the cutting forces, induced cutting damage, and machining parameters of CFRP composites

S. Zenia · L. Ben Ayed · M. Nouari · A. Delamézière

Received: 13 June 2014 / Accepted: 16 November 2014 / Published online: 7 December 2014

Abstract The use of carbon fiber reinforced polymer (CFRP) composites becomes more attractive today in various industrial sectors such as aerospace, naval, and automotive. This is due to their high mechanical properties (strength, stiffness, light weight, etc.) and corrosion resistance. Machining processes such as trimming or drilling are frequently used to achieve dimensional tolerance and assembly requirements. However, a damage process involving matrix cracking, fiber fracture, and interlaminar delamination often occurs when machining these materials. In the current work, a numerical analysis has been used to identify the most significant machining factors and their interaction on the induced damage and cutting force. The orthogonal Design of Experiments (DoE) $L_{27}(3^{13})$ of Taguchi has been applied to investigate the effect of the fiber orientation, the tool rake angle, the depth of cut, and the tool edge radius. The induced damage can strongly affect the surface roughness (surface quality of the workpieces) and considerably limits the use of these materials in many industrial applications. First of all, a coupled elastoplastic damage behavior law was adopted to simulate the permanent deformations caused by plasticity and to predict the degradation of mechanical properties due to the initiation of damage and its progression inside the composite structure. Satisfactory numerical results have been found and a good correlation has been obtained compared to experimental trends. The results reveal that the interaction between some factors could be neglected and the obtained responses are greatly influenced by the fiber orientation and the depth of cut rather than the tool rake angle and the tool edge radius.

S. Zenia · L. Ben Ayed · M. Nouari (✉) · A. Delamézière
Laboratoire d'Energétique et de Mécanique Théorique et Appliquée, LEMTA CNRS-UMR 7563, Ecole des Mines d'Albi, Université de Lorraine, GIP-InSIC, 27 rue d'Hellieule, 88100 Saint-Dié-des-Vosges, France
e-mail: mohammed.nouari@univ-lorraine.fr

Keywords Composite · Machining · Modeling · Taguchi method · Induced damage

Nomenclature

Cutting parameters

V_c	Cutting speed (m/min)
a_P	Depth of cut (mm)
α	Tool rake angle (°)
γ	Clearance angle (°)
F_c	Cutting force component (N)
F_t	Thrust force component (N)
μ	Friction coefficient

Mechanical quantities

σ	Cauchy stress tensor (MPa)
$\tilde{\sigma}$	Effective stress (MPa)
D	Macroscopic effect of the mechanical behavior degradation
F	Yield function (MPa)
f^p	Plastic potential
σ_y	Current yield stress (MPa)
p	Cumulated plastic strain
R_0	Initial yield stress (MPa)
α, β	Hardening parameters
c	Coupling parameter
$d\varepsilon$	Strain increment
$d\varepsilon^e$	Elastic strain increment
$d\varepsilon^p$	Plastic strain increment
$d\sigma$	Stress increment
C	Elastic stiffness matrix
E_i^0	Initial elastic modulus of a ply in the i direction (MPa)
ν_{12}^0	Poisson's ratio in the plane 12
G_{ij}^0	Initial shear modulus of a ply in the i–j plane (MPa)
$\tilde{\varepsilon}^p$	Effective plastic strain
λ	Plastic multiplier

W^p	Plastic work
U_x	Displacement along the x-axis
U_y	Displacement along the y-axis
ρ	Density (kg/m^3)

Damage quantities

e_D	Strain energy density of a ply
D_{22}, D_{12}	Matrix cracking and fiber–matrix debonding damage variables
Y_n	Thermodynamic force associated with the damage variable D_n (MPa)
Y^t_{11}	Limit strength for fiber damage in tension (MPa)
Y^c_{11}	Limit strength for fiber damage in compression (MPa)
Y^c_{12}	Limit strength for damage (MPa)
Y^0_{12}	Threshold strength for the initiation of damage (MPa)
b and b'	Coupling terms between the transverse and shear damage
τ_c	Characteristic time (μs)

1 Introduction

Generally, manufactured parts made from composite materials are designed directly to the desired shape through a more or less perfect process. It is often necessary to complete the overall shaping by finishing operations such as turning, milling, or drilling. However, the heterogeneity and the abrasive nature of fibers make the machinability of these materials more difficult compared to the conventional metals and their alloys. That is why the machining process of composites is considered today as a challenging task to manufacturing engineers, and several research works have been published aiming to evaluate the effect of the cutting parameters on the machinability of composites reinforced with carbon, glass, or aramid fibers [1–3]. Moreover, excessive tool wear and induced cutting damage in the workpiece such as the pullout of fibers, matrix cracking, and matrix–fiber debonding often occur when machining this kind of materials. Koplev et al. were the first authors [4, 5] to study the mechanisms of chip formation. They conducted several tests under orthogonal cutting configuration of CFRP composites. The main conclusion of their work is that the fiber orientation plays a key role in the chip formation process. Other machining tests were conducted by Wang et al. [6], Bhatnagar et al. [7], and Arola et al. [8] on edge trimming and orthogonal cutting of graphite/epoxy composites. These authors found that all aspects of composite materials removal were primarily dependent on the fiber orientation. It has been concluded from their works that the chip formation, the cutting force, and the surface morphology are highly controlled by the fiber orientation. Optimization based only on experimental approaches often requires long and expensive trials. So, numerical simulation and theoretical modeling can be very helpful to characterize and to validate optimal domains for the cutting parameters.

The Design of Experiments (DoE) allows us to optimize processes from a reliability viewpoint and product costs. In a domain such as machining, the use of the DoE method can be of great help in terms of reliability and product cost. Enemuoh et al. [9] studied the drilling process of carbon fiber reinforced thermoset laminates (BMS 8-256). They have used an approach based on a combination of Taguchi's technique and a multi-objective optimization criterion to identify the optimum drilling conditions and to study the influence of the drilling parameters such as cutting speed, feed rate, and tool point angle on the drilling performance measures: delamination, damage width, surface roughness, and drilling thrust force. They concluded that high cutting speed and low drilling feed rate are recommended for the production of delamination-free and good surface finish holes in epoxy composites. An approach based on the Taguchi method and the gray relational analysis was used by Palanikumar [10] to optimize the drilling parameters taking into account multiple quality characteristics, such as thrust force, workpiece surface roughness, and delamination. The obtained results show that a low feed rate and a high spindle speed improves the performances of drilling process of glass fiber reinforced polymer composite. To achieve a better surface roughness using the turning process, an experimental investigation based on Taguchi method was conducted by Rajasekaran et al. [11] in order to find the best combination parameters, such as cutting speed, feed, and depth of cut. They reported that the surface roughness will be reduced by increasing the cutting speed and improved using a higher feed rate. Pang et al. [12] worked on the optimization of machining parameters for end-milling operations applied to the hybrid composite material (HNT-AL/epoxy). The studied parameters are depth of cut, cutting speed, and feed rate. The obtained results show that through Taguchi's method, the authors succeeded to find the more appropriate combination of parameters that provide the optimal machining response.

To gain insight into the physics that governs the chip formation process, and interactions between the mechanical behavior and cutting parameters, expensive trials are often required. So, the finite element method has become an indispensable tool to analyze the cutting process and study the most influential parameters. The literature shows that many authors have proposed computational methods for composite damage and fracture. The majority of them are based on static or dynamic, implicit or explicit approaches, using shell or solid elements and considering macro-, meso-, micro-, or nano-mechanical models. Some of these models can be very precise but lead to very high computational times and need expensive computer resources.

From the last 10 years, relatively few numerical studies for machining process have been developed. Modeling the orthogonal cutting process for composites was firstly developed by Arola and Ramulu [13–15]. They proposed a simplified FE model based on failure criteria, the assumption of a homogeneous equivalent material (HEM) and the use of dual fracture process, to gain insight into the effects of the cutting tool geometry and fiber orientation on the material removal process. The predicted results (chip formation process and subsurface damage) could be enhanced because the fracture path was imposed and their model is based only on a purely elastic behavior. Ramesh et al. [14] developed a numerical method based on an elastoplastic theory and the total Lagrangian formulation to simulate the machining of FRPs. Lasri et al. [16] used a macro-mechanical approach to study the orthogonal cutting of unidirectional glass fiber reinforced polymer (GFRP). Their FE model is based on the concept of stiffness degradation, and three failure criteria were considered: Hashin, Maximum Stress, and Hoffman. These criteria have been implemented for a 2D numerical model using the user subroutine USDFLD [17] to study the chip formation process, machining forces, and damage modes such as matrix cracking, fiber–matrix debonding, and fiber breaking. It was shown that the use of the stiffness degradation concept with an appropriate failure criterion allows to simulate the chip formation process for machining of FRPs. This method has the advantage of simplicity for the numerical implementation and the drawback of this approach, which is governed by an appropriate stiffness change which is in fact not known. In addition to the difficulty related to the definition of the appropriate stiffness change, there is the problem related to stress concentrations which can sometimes give problems of convergence; in other words, it is difficult to reachieve equilibrium after degradation. A micro-mechanical model, with fiber assumed elastic and the matrix elastoplastic, was proposed by Rao et al. [18] to estimate the cutting forces during orthogonal machining of unidirectional CFRP and GFRP composites. The workpiece was divided into two areas. The first area is close to the tool, in which fiber and matrix have been modeled separately, and the second area is away from the tool, in which the authors consider a HEM. The fiber–matrix interface was modeled with zero thickness cohesive elements. The damage in the matrix is assumed to be isotropic and is governed by an appropriate degradation of elastic properties once a yielding stress is reached. In summary, the analyses carried out without any special regularization scheme are, in general, mesh dependent. This is a common characteristic of all softening models used in FE computations, in particular for those simulating a very brittle behavior.

In this work, the DoE method was applied to study the effect of some machining parameters on the cutting force and induced damage. The aim of this study is to find the optimal combination of machining parameters providing the best machining responses according to the cutting force and subsurface damage. In the current investigation, a FE model based on a combined elastoplastic damage constitutive law was used to study the machining process. The model allows a better understanding of the physical phenomena observed during the cutting operation and gives an accurate numerical tool to simulate the real chip formation, cutting force, and induced subsurface damage. To avoid numerical localization of damage, regularization parameters are used for the damage variables. Satisfactory results have been obtained on an orthogonal cutting test and a good correlation has been shown compared to experimental data given in [6, 7, 19–21] and numerical results taken from [13–16, 18, 22–30]. The FE model was coupled with the Taguchi method to study the impact of the machining parameters on the cutting force and induced subsurface damage.

2 Combined elastoplastic damage behavior for CFRP composites in machining

In the current study, the effective stresses concept has been adopted [31]. The yield function is written considering an isotropic hardening and no plastic flow is assumed in the fiber direction. Let us consider a unidirectional fiber-reinforced lamina in the reference frame of Fig. 1. (1) denotes the fiber direction; (2), the plane direction orthogonal to fibers; and (3), the direction normal to the layer plane.

The layer is assumed to be in a plane stress situation, i.e., only σ_{11}, σ_{22}, and σ_{12} are nonzero stresses.

2.1 Plasticity effects

The elasticity domain is defined according to the following plastic activation function:

$$F\left(\widetilde{\boldsymbol{\sigma}}, \sigma_{\mathrm{y}}\right) = f^{p}\left(\widetilde{\boldsymbol{\sigma}}\right) - \sigma_{\mathrm{y}}(p) \tag{1}$$

where f^{p} is the plastic potential and σ_{y} is the current yield stress which represents the isotropic hardening law and it is defined in function of the cumulated plastic strain p

$$\sigma_{\mathrm{y}}(p) = R_0 + R(p) = R_0 + \beta p^{\alpha} \tag{2}$$

where R_0 is the initial yield stress and the quantities β and α are the hardening parameters.

The plastic potential function is defined considering a plane stress condition, and it does not depend on stresses σ_{11} in the fiber direction because the fiber behavior is assumed to be elastic brittle under tension or compression:

$$f^{p}\left(\widetilde{\sigma}\right) = \sqrt{\widetilde{\sigma}_{12}^{2} + c^{2}\widetilde{\sigma}_{22}^{2}} \tag{3}$$

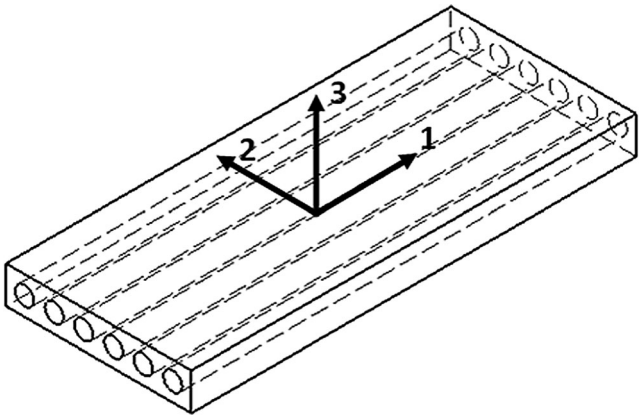

Fig. 1 Composite layer: *1* fiber orientation, *2* transverse orientation, and *3* direction normal to the layer plane

where c is a coupling parameter and the effective stresses are defined as follows:

$$\widetilde{\sigma}_{12} = \frac{\sigma_{12}}{1-D_{12}}; \widetilde{\sigma}_{22} = \frac{\langle \sigma_{22} \rangle_+}{1-D_{22}} + \langle \sigma_{22} \rangle_- \tag{4}$$

where D_{22} and D_{12} denote damage developed in the transverse direction and under shear stress condition, respectively. The symbols $\langle \bullet \rangle_-$ and $\langle \bullet \rangle_+$ in Eq. (4) mean the negative and positive part of •, respectively, introduced to model the unilateral effect for the effective transverse stress. The transverse behavior in compression is indefinitely elastoplastic due to the introduced unilateral effect. So, transverse damage affects only the tensile behavior.

At each iteration time and for each integration point, a strain increment $\{\mathbf{d\varepsilon}\}$ is computed and additively decomposed into elastic and inelastic parts:

$$\{\mathbf{d\varepsilon}\} = \{\mathbf{d\varepsilon}^e\} + \{\mathbf{d\varepsilon}^p\} \tag{5}$$

The stress increment is given by the generalized Hooke's law as:

$$\{\mathbf{d\sigma}\} = [\mathbf{C}](\{\mathbf{d\varepsilon}\} - \{\mathbf{d\varepsilon}^p\}) \tag{6}$$

where $[\mathbf{C}]$ is the elastic stiffness matrix:

$$C = \begin{bmatrix} \frac{(1-D_{11})}{1-\nu_{12}^0\nu_{21}^0} E_{11}^0 & \frac{\nu_{12}^0(1-D_{22})}{1-\nu_{12}^0\nu_{21}^0} E_{22}^0 & 0 \\ \frac{\nu_{12}^0(1-D_{22})}{1-\nu_{12}^0\nu_{21}^0} E_{22}^0 & \frac{(1-D_{22})}{1-\nu_{12}^0\nu_{21}^0} E_{22}^0 & 0 \\ 0 & 0 & (1-D_{12})G_{12}^0 \end{bmatrix} \tag{7}$$

E_{11}^0, E_{22}^0 are the undamaged Young's moduli for directions 1 and 2, G_{12}^0 is the undamaged shear modulus in the plane 12, and the Poisson's ratios in the plane 12 are ν_{12}^0 and ν_{21}^0 . D_{11} is the damage variable in the fiber direction.

When the material deforms elastically, the elastic strain part is equal to the total strain increment ($\{\mathbf{d\varepsilon}\} = \{\mathbf{d\varepsilon}^e\}$) and the inelastic strain increment vanishes. The effective inelastic part of the deformation is defined by the flow rule (or normality rule) as:

$$\left\{\mathbf{d}\tilde{\boldsymbol{\varepsilon}}^p\right\} = \mathrm{d}\lambda \frac{\partial F}{\partial\left\{\tilde{\boldsymbol{\sigma}}\right\}} \text{ and } \mathrm{d}p = -\mathrm{d}\lambda \frac{\partial F}{\partial \sigma_y} = \mathrm{d}\lambda \tag{8}$$

where $\mathrm{d}\lambda$ is a nonnegative plastic consistency parameter (plastic multiplier).

The plastic strain increment is obtained from the equivalence principle of the plastic work increment $\mathrm{d}W^p$ presented as follows:

$$\mathrm{d}W^p = \tilde{\boldsymbol{\sigma}} : \mathbf{d}\tilde{\boldsymbol{\varepsilon}}^p = \boldsymbol{\sigma} : \mathbf{d}\boldsymbol{\varepsilon}^p \tag{9}$$

In addition, the consistency condition ($\mathrm{d}F=0$) should be satisfied and leads to compute the cumulated plastic increment:

$$\mathrm{d}p = \frac{\left\langle \frac{\partial F}{\partial \tilde{\boldsymbol{\sigma}}} \right\rangle [\mathbf{C}]}{\left\langle \frac{\partial F}{\partial \tilde{\boldsymbol{\sigma}}} \right\rangle [\mathbf{C}] \left\{ \frac{\partial F}{\partial \tilde{\boldsymbol{\sigma}}} \right\} + \frac{\partial \sigma_y}{\partial p}} \{\mathbf{d\varepsilon}\} = \langle \mathbf{a} \rangle \{\mathbf{d\varepsilon}\} \tag{10}$$

The stress increment (6) could be computed using relations (8), (9), and (10). Finally, the updated stress vector should satisfy the second consistency condition ($F=0$). An algorithm based on a radial returns predictor [32] is implemented in order to return the stresses to the yield surface. In fact, for an increment strain, an initial elastic prediction step is carried out. If the yield function is greater than zero, an iterative correction procedure uses the normal of the last yield surface until the yield function vanishes.

2.2 Damage analysis

Different degradation modes are considered in the FE analysis: fiber breakage in tension as well as in compression, matrix cracking, and fiber–matrix debonding. In the 2D configuration, the strain energy density of the damaged ply is defined as follows [33–35]:

$$e_D = \frac{1}{2}\left[\frac{\sigma_{11}^2}{E_{11}^0(1-D_{11})} - \frac{2\nu_{12}^0}{E_{11}^0}\sigma_{11}\sigma_{22} + \frac{\langle \sigma_{22} \rangle_+^2}{E_{22}^0(1-D_{22})} + \frac{\langle \sigma_{22} \rangle_-^2}{E_{22}^0} + \frac{\sigma_{12}^2}{G_{12}^0(1-D_{12})}\right] \tag{11}$$

This equation shows which terms of the stiffness are influenced by the damage. To describe the initiation and

progression of degradation mechanisms, the thermodynamic force vector **Y** conjugated to damage is used:

$$\mathbf{Y} = \frac{\partial \langle\langle e_D(\boldsymbol{\sigma}, \mathbf{D}) \rangle\rangle}{\partial \mathbf{D}} \tag{12}$$

Where the symbol $\langle\langle \bullet \rangle\rangle$ in Eq. (12) means the average value of the quantity • within the thickness. In the present study, the strain energy density is computed locally at each integration point across the ply thickness.

The activation of damage and its evolution is governed by the square root of a linear combination of the two thermodynamic forces Y_{22} and Y_{12}:

$$\overline{Y} = \sup_{\tau \le t} \left(\sqrt{Y_{12} + bY_{22}} \right) \tag{13}$$

where b is a coupling term between the transverse and shear forces. The variables Y_{22} and Y_{12} are defined according to (12):

$$Y_{22} = \frac{\langle \sigma_{22} \rangle_+^2}{2(1-D_{22})^2 E_{22}^0} \tag{14}$$

$$Y_{12} = \frac{\sigma_{22}^2}{2(1-D_{12})^2 G_{12}^0}$$

The transverse and shear damage variables D_{22} and D_{12} are defined as:

$$\Rightarrow D_{12} = \begin{cases} \dfrac{\left\langle \sqrt{\overline{Y}} - \sqrt{Y_{12}^0} \right\rangle_+}{\sqrt{Y_{12}^c} - \sqrt{Y_{12}^0}}, & \text{if } D_{12} < 1 \text{ and } Y_{12} < Y_{12}^c \\ 1 & \text{otherwise} \end{cases} \tag{15}$$

$$\Rightarrow D_{22} = \begin{cases} b' D_{12}, & \text{if } D_{22} < 1 \text{ and } Y_{22} < Y_{12}^c \\ 1 & \text{otherwise} \end{cases} \tag{16}$$

where b' is a coupling term between the transverse and shear damages. Y_{12}^c and Y_{12}^0 are the limit strength for damage and the threshold strength for the initiation of damage, respectively. These material parameters are identified experimentally.

In addition to the above equations, the model is completed by a brittle failure criterion which takes into account failure of the fiber in tension and compression. This is governed by two critical damage thresholds Y_{11}^t and Y_{11}^c for the variable Y_{11}:

$$Y_{11} = \frac{\sigma_{11}^2}{2(1-D_{11})^2 E_{11}^0} \tag{17}$$

The damage fiber is introduced in the model, by considering Young's modulus E_{11} as nonlinear and depending on stresses σ_{11}:

$$\begin{cases} \text{if } \sigma_{11} > 0 \rightarrow \begin{cases} \text{if } Y_{11} > Y_{11}^t \ D_{11} = 1 \\ \text{otherwise } D_{11} = 0 \end{cases} \\ \text{if } \sigma_{11} < 0 \rightarrow \begin{cases} \text{if } Y_{11} > Y_{11}^c \ D_{11} = 1 \\ \text{otherwise } D_{11} = 0 \end{cases} \end{cases} \tag{18}$$

To limit the maximum damage rate and avoid numerical localization of damage, regularization parameters are introduced [36, 37]. Then, the damage variables are corrected as below:

$$D_{ij} = \frac{1}{\tau_c} \left(1 - e^{-a \left(D_{ij}^s - D_{ij} \right)} \right) \tag{19}$$

The same material constants, τ_c and a, are taken for the three damage evolution laws. For this model with delay effects, the variations of the forces Y_i do not lead to instantaneous variations of the damage variables D_i. There is a certain delay, defined by the characteristic time τ_c.

The nonlinear and irreversible constitutive laws presented previously were implemented in Abaqus/Explicit finite element software through the user subroutine VUMAT. The formulation history is discretized into a sequence of time interval $[t_n, t_{n+1}]$. Here, the subscript n or $n+1$ means a quantity computed at time instant t_n or t_{n+1}, respectively. The plastic activation function (1), the hardening law (2), the stress–strain increment relationship (6), and the plastic flow rule (8) represent the main relationships of the nonlinear plastic constitutive model. The procedure is described in the flowchart of Fig. 2.

3 Numerical simulation of the machining process

In this section, an orthogonal cutting operation is investigated and the results carried out with the proposed FE model are compared to experimental results taken from the work of Iliescu et al. [27]. The same application is used in Section 4 with the Taguchi method to optimize the machining operation.

3.1 Setup of the finite element calculation

Geometry and boundary conditions of the machining application are illustrated in Fig. 3. Nodes on the vertical lines, right and left sides, are constrained to move along the horizontal direction (X). Nodes on the horizontal bottom line are restrained to move along the horizontal and vertical directions (X) and (Y), respectively. The geometrical parameters of the workpiece and the tool are shown in Fig. 3. The cutting speed V_c is equal to 60 m/min. The tool is modeled as a rigid body

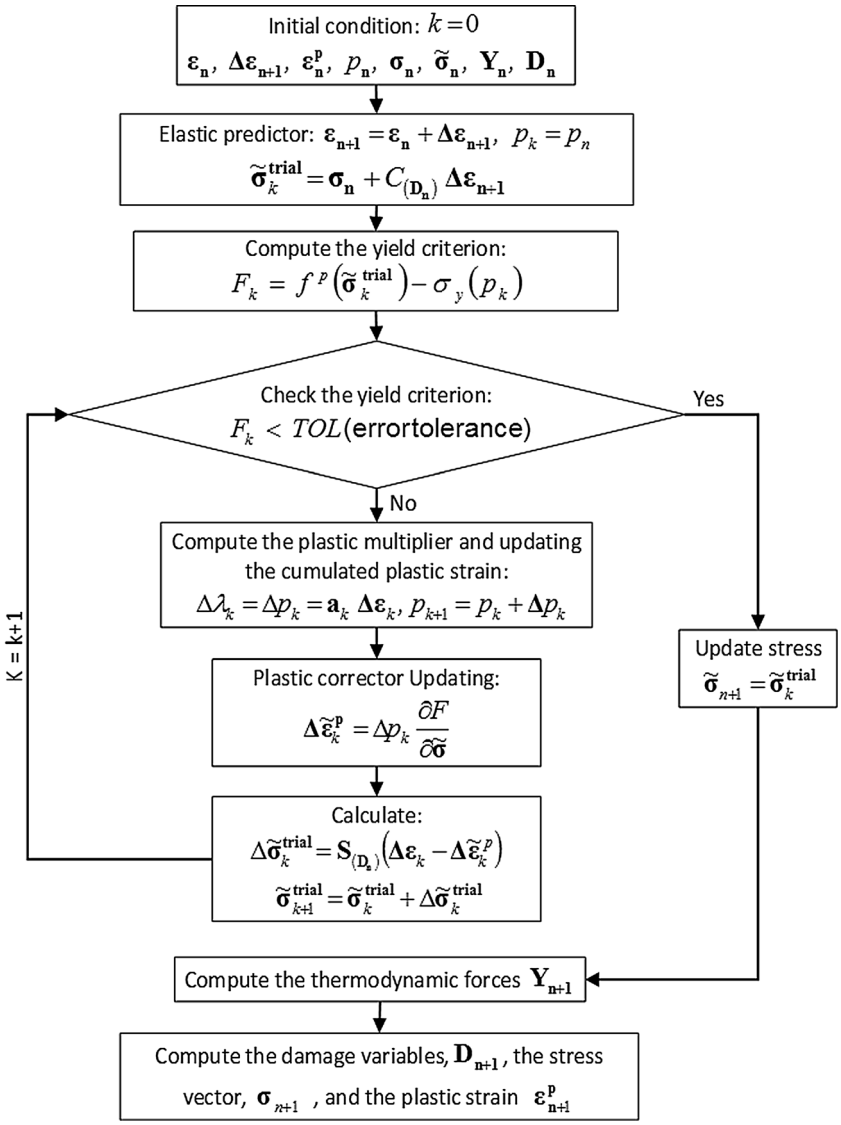

Fig. 2 Flow chart of the implemented user subroutine VUMAT

and controlled by a reference point, where the cutting speed is applied and the machining forces are measured.

The mechanical properties of the CFRP ply of T300/914 are taken from the work of Iliescu et al. [27] and remembered in Table 1. The workpiece is considered as a homogeneous equivalent material with a longitudinal modulus in the fiber direction more than ten times higher than the transverse modulus.

The numerical simulation is carried out using a dynamic explicit approach of Abaqus software [17]. A 2D model is conducted considering plane stress assumption and using a linear continuum solid elements CPS4R including automatic hourglass control with reduced integration.

The mesh size was defined to achieve both accuracy and time efficiency of the calculation. As shown in Fig. 3, the near zone of the tool where the chip will be formed was finely meshed with an element size of 5 μm, while the remaining part was meshed coarsely with an element size of 5 μm, in the vicinity of the finely meshed area, and 50 μm on the other edges.

A VUMAT subroutine providing a very general capability for implementing elastoplastic damage models was used. In addition, the element deletion approach is applied to represent the process of chip formation based on initiation and damage evolution in the workpiece. The set of the plastic-damage model parameters reported by Feld [38] have been adopted for all simulations in this work (see Table 2).

The interaction between the node set of the workpiece surface and the tool surface is modeled using surface-to-surface contact algorithm coupled to kinematic predictor/corrector contact algorithm with finite sliding formulation which are available in Abaqus/Explicit package. This approach allows to correctly manage the contact between the tool and the workpiece and this in spite the use of the "element deletion" option that eliminates the elements for which the

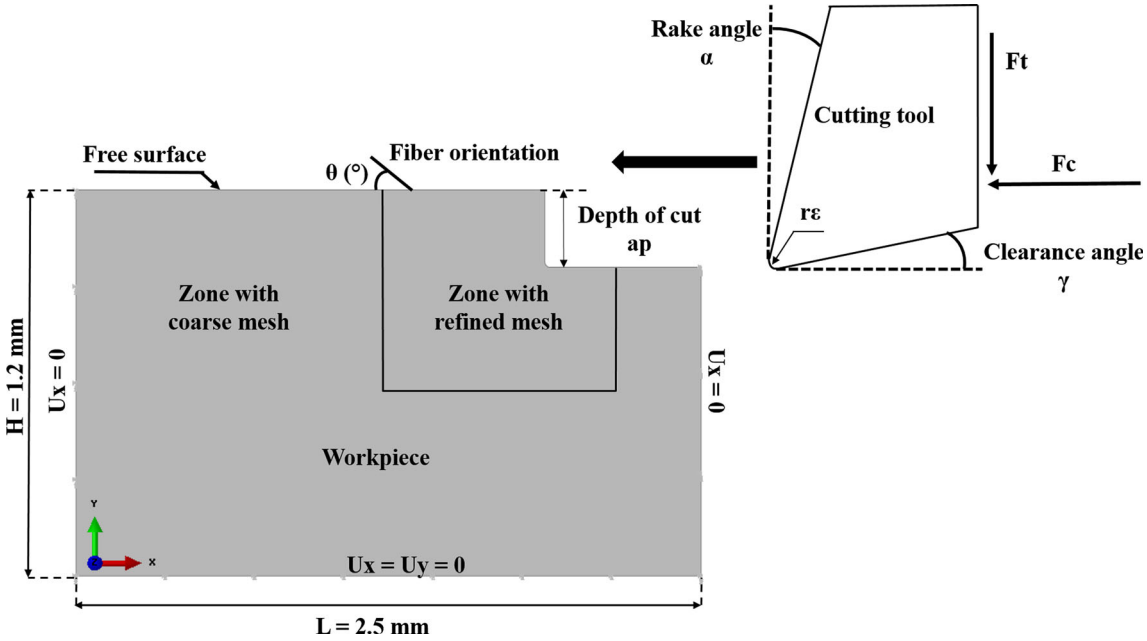

Fig. 3 Boundary condition and dimensions of the workpiece and the cutting tool

damage is too large. In fact, the contact zone between the tool and the workpiece is continually updated with the movement of the tool along its path and the workpiece evolution due to the removal of the damaged elements. This allows to have easily the complete chip formation process, as in various numerical studies, Nayak et al. [24], Rao et al. [18], Lasri et al. [26], and Santiuste et al. [28]. The interaction between surfaces (tool/workpiece) is controlled by the Coulomb friction law and the friction coefficient, μ, which is assumed to be constant during the cutting operation and equal to 0.4.

3.2 Numerical results

The numerical results obtained by the FE model were made using the same machining condition used in the work of Iliescu et al. [27]. These authors conducted orthogonal cutting experiments on CFRP composites and investigated the effect of the fiber orientation on cutting force and chip formation. The mechanical properties used here are reported in Table 2. The used machining conditions (tool geometry, cutting speed, and boundary conditions) are the same introduced in Section 3.1. Figure 4 shows the cutting force carried out using the proposed FE model and also the experimental results. Numerical cutting forces are calculated at each time increment during the cutting operation. The collected data are relatively noisy due to the high frequency variation of forces, which is an inherent characteristic of composite machining due to the repeated fiber/matrix fracture to form discontinuous chips. They are refined by a median filter developed on Matlab, whose cutting of frequency is adjusted according to the noise level, in order to facilitate their use. The effect of the fiber orientation on cutting force is highlighted by Fig. 4. The conclusion that can be drawn from this graph is that the fiber orientation affects significantly the cutting force. It can be observed that the cutting force registers a minimum in the [0° 45°] fiber orientation range and increased thereafter up to

Table 1 Mechanical properties of the aeronautical CFRP composite T300/914

Mechanical properties	
E_1^0(MPa)	136,600
E_2^0(MPa)	9600
G_{12}^0(MPa)	5200
ν_{12}^0	0.29
ρ (kg/m^3)	1578

Table 2 Plastic and damage parameters of UD-CFRP T300/914

Damage parameters	
Y_{12}^c(MPa)	8
Y_{12}^0(MPa)	0.03
b	0.5
b'	0.8
Y_{11}^t(MPa)	15
Y_{11}^c(MPa)	12
a	1
τ_c(μs)	6
Plastic parameters	
α	0.54
β (MPa)	1000
c	0.7
R_0 (MPa)	64

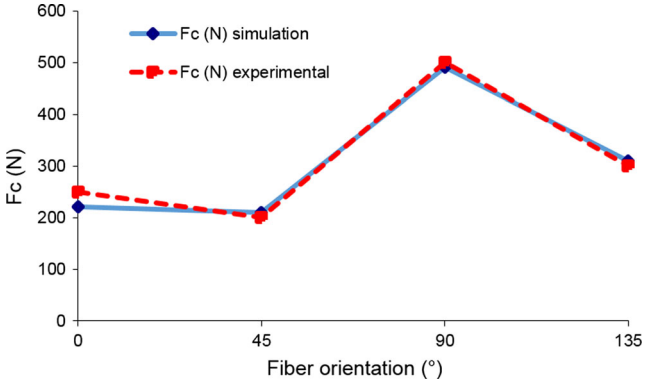

Fig. 4 Numerical and experimental [27] results of the cutting force for different fiber orientations

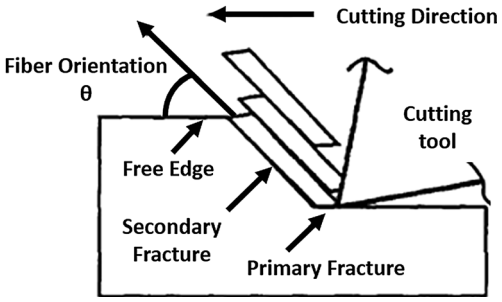

Fig. 6 Schematization of the experimental observation of the chip formation under orthogonal cutting configuration for 45° fiber orientation [8]

90°. The numerical results, carried out using the proposed FE modeling for different fiber orientations, are in good agreement with the experimental results (Figs. 4, 5, 6 and 7).

Figure 5 shows the chip formation mechanisms for the fiber orientation of 45°. The subfigures a, b, c, and d present the damage evolution during the machining operation for different time steps: 4×10^{-6}, 1.32×10^{-4}, 2.76×10^{-4}, and 2.82×10^{-4} s. The damage is followed from the initiation and progression stage to the complete chip formation stage. The chip formation mechanisms were composed of a primary fracture across the fiber axis followed by a secondary fracture along the fiber–matrix interface. The numerical results show that the elastoplastic damage FE model reproduces the chip formation process observed experimentally by Arola et al. [8] in Fig. 6. Also, the same conclusion was drawn regarding the results in Fig. 7.

An important point of this work concerns the formation of the real chip (see Fig. 7). Note that the chip formation process for composites is not easy to realize as for the case of metallic alloys because of the different chip morphologies that can be obtained (powder chips, long and continuous chips, or

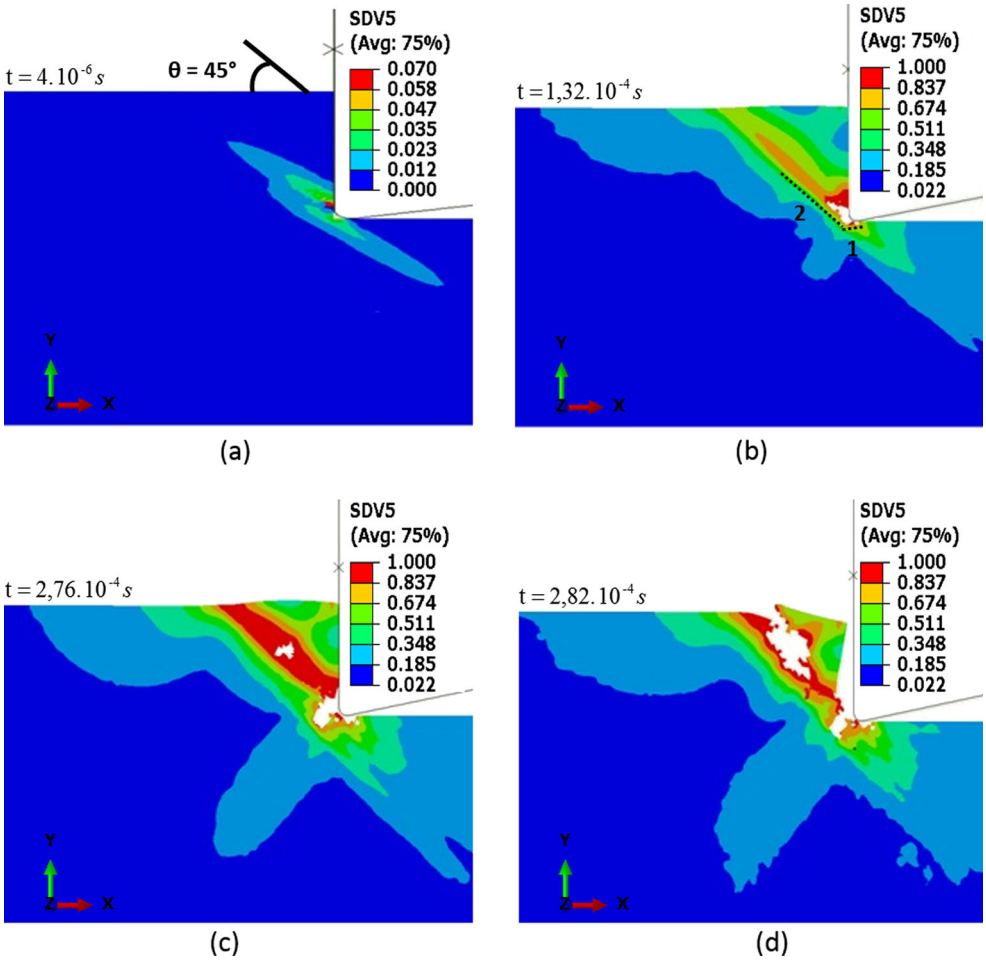

Fig. 5 Progressive failure analysis of the formed chip for 45° fiber orientation

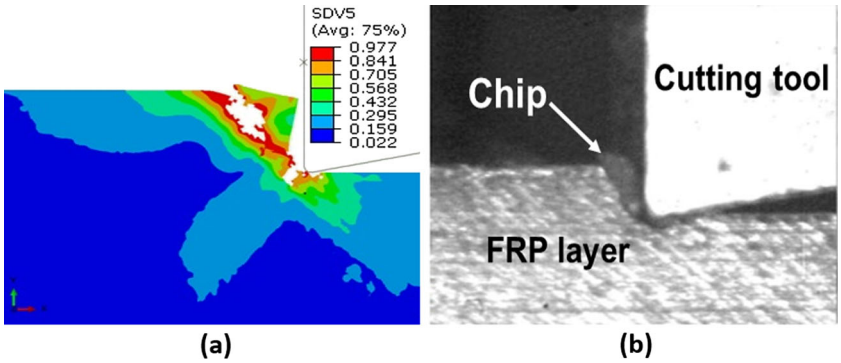

Fig. 7 Chip formation in orthogonal cutting of unidirectional composite at 45°: **a** numerical result, **b** high-speed video image from experiment work of Iliescu et al. [27]

fragmented chips). This is due to the anisotropy and the heterogeneity of this material.

Besides, Fig. 4, in which numerical and experimental [27] results of cutting forces for different fiber orientations are reported, shows that cutting forces obtained with the proposed model are in good agreement with the experimental results of Iliescu et al. [27], and this is true for different fiber orientations.

3.3 Taguchi method

Design of Experiments [12, 39] is a powerful tool to provide complex information such as the interaction between cutting factors and composite behavior in the machining process. This method allows to find the best combination of design parameters with a minimum number of analyses. The orthogonal arrays (OA) form the basis for the experimental/numerical analysis in the Taguchi method. After conducting the analyses according to an OA and determining the effect each factor has on the response, the signal-to-noise (S/N) ratio is calculated for each conducted analysis. The "Lower is better" (LB) characteristic is chosen to achieve the lowest subsurface damage and cutting force values.

lower is better (LB):

$$\mathrm{S/N\ ratio} = -10\log_{10}\left[\frac{1}{r}\sum y^2\right] \tag{20}$$

where r is the number of observations, r the observed data, $\bar{y}$ the average observed data, and σ the variance of y.

In this study, four independent parameters (fiber orientation, tool rake angle, tool edge radius, and depth of cut) were selected and a standard (OA) $L_{27}(3^{13})$ was employed. The OA $L_{27}(3^{13})$ is chosen due to its capability to check the interactions among the factors, and it makes use of three levels for each. Taguchi's table is associated to one or more linear graphs ready to be used [39].

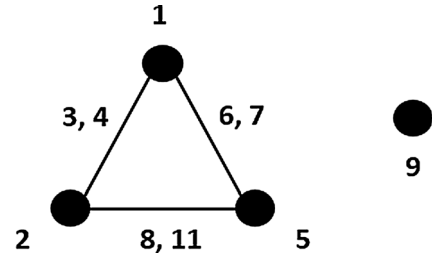

Fig. 8 Linear graph for L27 array

The chosen factors could be partitioned into four groups according to the difficulty encountered to update the FE model when changing factor level, from easiest to difficult to change. In this numerical study, it can be considered that the four factors subjected to the analysis are easy to change. Therefore, all factors are taken as being easy to change. As shown in Fig. 8, a linear graph is used to assign the factors and interactions to various columns of the orthogonal array. Table 3 indicates the factors and levels in machining test. Factors A, B, C, and D are arranged in columns 1, 2, 5, and 9, respectively, in the standard L_{27} (3^{13}) orthogonal array as shown in Table 4.

The plan of the experiments (numerical tests) is as follows: the first column is assigned to fiber orientation (A), the second column to tool rake angle (B), the fifth column to tool edge radius (C), and the eighth column to depth of cut (D); the third and fourth columns are assigned to $(AB)_1$ and $(AB)_2$, respectively, to estimate interaction between fiber orientation (A) and tool rake angle (B); the sixth and seventh columns are assigned to $(AC)_1$ and $(AC)_2$, respectively, to estimate interaction between fiber orientation (A) and tool edge radius (C); the ninth and 11th columns are assigned to $(BC)_1$ and $(BC)_2$, respectively, to estimate interaction between tool rake angle (B) and tool edge radius (C).

Table 5 summarizes different experimental works that have been interested in the machining optimization/calibration of composites. These works show the main factors influencing

Table 3 Levels of the variables used in the experiment

Control factor	Level			
	1	2	3	Units
A: Fiber orientation	15	45	75	°
B: Tool rake angle	−10	0	10	°
C: Tool edge radius	10	20	30	μm
D: Depth of cut	0.1	0.2	0.3	mm

Table 4 Orthogonal array for L_{27} (3^{13}) Taguchi design

Trial	1	2	3	4	5	6	7	8	9	10	11	12	13
	A	B	$(A\times B)_1$	$(A\times B)_2$	C	$(A\times C)_1$	$(A\times C)_2$	$(B\times C)_1$	D	–	$(B\times C)_2$	–	–
1	1	1	1	1	1	1	1	1	1	1	1	1	1
2	1	1	1	1	2	2	2	2	2	2	2	2	2
3	1	1	1	1	3	3	3	3	3	3	3	3	3
4	1	2	2	2	1	1	1	2	2	2	3	3	3
5	1	2	2	2	2	2	2	3	3	3	1	1	1
6	1	2	2	2	3	3	3	1	1	1	2	2	2
7	1	3	3	3	1	1	1	3	3	3	2	2	2
8	1	3	3	3	2	2	2	1	1	1	3	3	3
9	1	3	3	3	3	3	3	2	2	2	1	1	1
10	2	1	2	3	1	2	3	1	2	3	1	2	3
11	2	1	2	3	2	3	1	2	3	1	2	3	1
12	2	1	2	3	3	1	2	3	1	2	3	1	2
13	2	2	3	1	1	2	3	2	3	1	3	1	2
14	2	2	3	1	2	3	1	3	1	2	1	2	3
15	2	2	3	1	3	1	2	1	2	3	2	3	1
16	2	3	1	2	1	2	3	3	1	2	2	3	1
17	2	3	1	2	2	3	1	1	2	3	3	1	2
18	2	3	1	2	3	1	2	2	3	1	1	2	3
19	3	1	3	2	1	3	2	1	3	2	1	3	2
20	3	1	3	2	2	1	3	2	1	3	2	1	3
21	3	1	3	2	3	2	1	3	2	1	3	2	1
22	3	2	1	3	1	3	2	2	1	3	3	2	1
23	3	2	1	3	2	1	3	3	2	1	1	3	2
24	3	2	1	3	3	2	1	1	3	2	2	1	3
25	3	3	2	1	1	3	2	3	2	1	2	1	3
26	3	3	2	1	2	1	3	1	3	2	3	2	1
27	3	3	2	1	3	2	1	2	1	3	1	3	2

Table 5 Literature works in the field of machining optimization of FRP composites

Authors	Performed work	Conclusions
Wang et al. [6]	Experimental work on orthogonal cutting mechanisms of graphite/epoxy composite	The authors concluded in this work that the lowest resultant cutting force was measured when trimming 0° material with a rake angle α 10° tool
Arola et al. [8]	Chip formation in orthogonal trimming of graphite/epoxy composite	The chip formation is highly dependent on the fiber orientation
		A spectral analysis of the machined surface profiles indicated that the period of fracture during chip generation decreased with increasing rake angle of the tool inserts
Wang and Zhang [20]	Investigations on orthogonal cutting of cutting of unidirectional fiber reinforced plastics	The fiber orientation is a key factor that determines the surface integrity of a machined component. θ=90° is a critical angle, beyond which severe subsurface damage will occur
		The rake angle of a cutting tool, α, affects only slightly the surface roughness. In the range studied, a better surface will be obtained when α=20°
Nayak et al. [24]	Experimental work on damage of composites	The subsurface damage is found minimum for the fiber orientation 15°
		The effect of positive tool rake angle on the subsurface damage is not very significant for fiber orientations less than 45°

Table 6 Simulation results

Trial	Fiber orientation	Tool rake angle	Tool edge radius	Depth of cut	Cutting force	S/N	Induced damage	S/N
	A (°)	B (°)	C (μm)	D (mm)	(N/mm)	(dB)	(μm)	(dB)
1	15	−10	10	0.1	22	−26.85	11	−20.83
2	15	−10	20	0.2	45	−33.06	19	−25.58
3	15	−10	30	0.3	52	−34.32	20	−26.02
4	15	0	10	0.2	40	−32.04	18	−25.11
5	15	0	20	0.3	50	−33.98	19	−25.58
6	15	0	30	0.1	20	−26.02	14	−22.92
7	15	10	10	0.3	43	−32.67	19	−25.58
8	15	10	20	0.1	21	−26.44	14	−22.92
9	15	10	30	0.2	35	−30.88	18	−25.11
10	45	−10	10	0.2	48	−33.62	50	−33.98
11	45	−10	20	0.3	74	−37.38	65	−36.26
12	45	−10	30	0.1	34	−30.63	35	−30.88
13	45	0	10	0.3	57	−35.12	60	−35.56
14	45	0	20	0.1	31	−29.83	35	−30.88
15	45	0	30	0.2	47	−33.44	39	−31.82
16	45	10	10	0.1	28	−28.94	28	−28.94
17	45	10	20	0.2	41	−32.26	40	−32.04
18	45	10	30	0.3	55	−34.81	42	−32.46
19	75	−10	10	0.3	100	−40.00	130	−42.28
20	75	−10	20	0.1	40	−32.04	56	−34.96
21	75	−10	30	0.2	75	−37.50	77	−37.73
22	75	0	10	0.1	39	−31.82	43	−32.67
23	75	0	20	0.2	61	−35.71	65	−36.26
24	75	0	30	0.3	90	−39.08	119	−41.51
25	75	10	10	0.2	53	−34.49	80	−38.06
26	75	10	20	0.3	80	−38.06	102	−40.17
27	75	10	30	0.1	36	−31.13	49	−33.80
Fc Effects for means								
Level 1	−30.70	−33.93	−32.84	−29.30				
Level 2	−32.89	−33.00	−33.20	−33.67				
Level 3	−35.54	−32.19	−33.09	−36.16				
Delta	4.84	1.75	0.36	6.86				
Rank	2	3	4	1				
Dm effects for means								
Level 1	−24.40	−32.06	−31.44	−28.76				
Level 2	−32.54	−31.37	−31.63	−31.74				
Level 3	−37.49	−31.01	−31.36	−33.94				
Delta	13.09	1.05	0.27	5.18				
Rank	1	3	4	2				

the machining process of composites (cutting forces, damage, chip morphology, etc.). Thanks to these works, the parameters A, B, C, and D have been chosen.

According to other studies [7, 25, 27, 29], the cutting force and the subsurface damage are at their maximum levels when the fiber orientation is about 90°. Besides, cutting force and subsurface damage are at their lowest levels when the fiber orientation is about 0°. In the current study, the fiber orientation will varied in the range [15°, 75°], and three levels have been chosen: 15, 45, and 75°. For the rake angle factor, the chosen levels are −10, 0, and 10°. This was motivated according to the chip formation mechanisms observed during the cutting operation [6, 8, 18, 22]. Indeed, for a positive rake angle, the preponderant mechanism is

shearing, while with a negative rake angle the dominant mechanism is buckling. The ranges of variation, of the tool edge radius and the depth of cut factors, have been chosen according to several works [6, 7, 20, 25, 29, 30].

4 Results and discussion

The numerical results carried out according to the chosen Taguchi OA of 27 different combinations are reported in Table 6. The collected cutting forces are relatively noisy. They are refined by a median filter developed on Matlab code, whose cutting of frequency is adjusted according to the noise level, in order to facilitate their use as shown in Fig.9a.

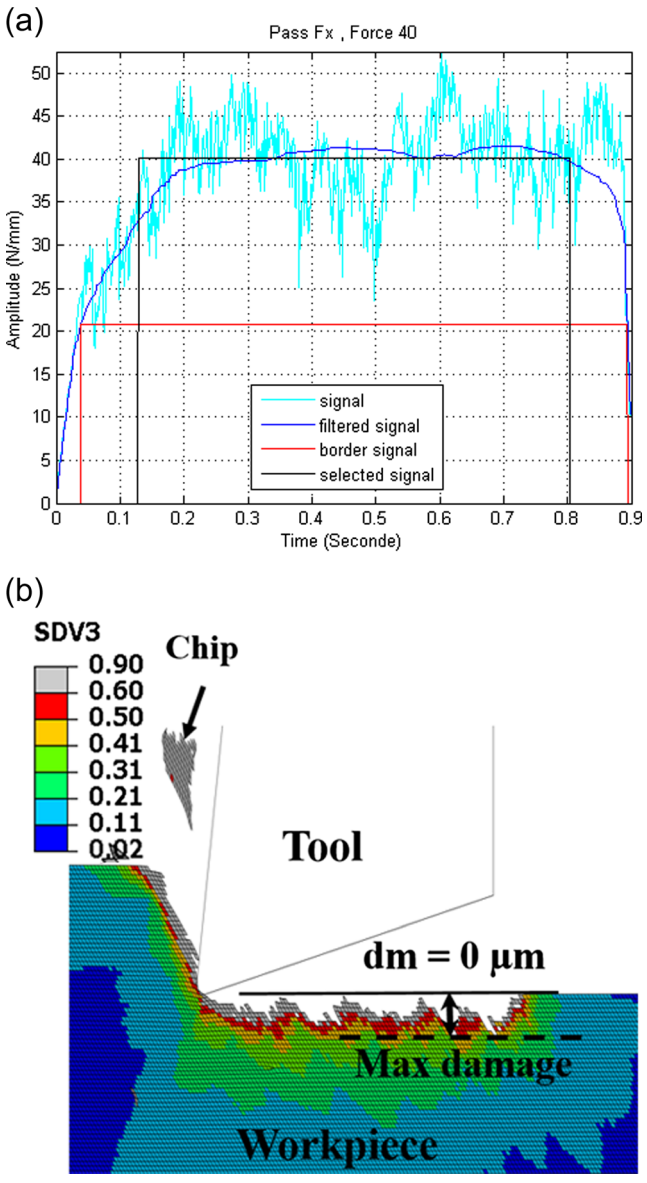

Fig. 9 Methods of measure: **a** cutting forces and **b** induced damage

Figure 9b shows the used method to measure the induced damage. The material is considered to be damaged when the damage value exceeds 60 %. In this table, "Delta" indicates the difference between the maximum and minimum average value of the response at particular level. "Rank" indicates the level of influence of parameters. From the analysis of the table, it has been asserted that fiber orientation and depth of cut are the highly influential parameters which affect the responses in cutting of CFRP composites.

4.1 Estimation of effects and interactions of the factors

The arithmetic mean of all responses, y_i, concerning cutting force "*Fc*" and damage "*dm*", are estimated as follows:

$$m = \frac{\sum_{i=1}^{27} y_i}{27} \tag{21}$$

where i is the experiment number.

The effect of a given factor, A, at level k on the response is calculated by the following formula:

$$a_k = \overline{y(A_k)} - m \tag{22}$$

where $a_k = \overline{y(A_k)} - m$ is the arithmetic mean evaluation of factor A, when its level is fixed at "k":

$$\overline{y(A_k)} = \frac{\sum_{1 \le i \le r(A_k)} y_i(A_k)}{r(A_k)} \tag{23}$$

where $r(A_k)$ is the number of evaluations associated to A at its level k.

On the other hand, the estimation of interaction terms of factors, A and B, is done as follows:

$$(ab)_{kl} = \overline{y(A_k; B_l)} - m - a_k - b_l \tag{24}$$

where $\overline{y(A_k; B_l)}$ is the arithmetic mean of factors, A and B, on the response when their levels are fixed at k and l, respectively:

$$\overline{y(A_k; B_l)} = \frac{\sum_{1 \le i \le r(A_k; B_l)} y_i(A_k; B_l)}{r(A_k; B_l)} \tag{25}$$

where $r(A_k; B_l)$ is the number of evaluations associated with the parameters A and B at their levels k and l, respectively.

4.2 Analysis of effects and interactions of factors

The mean of means and of S/N ratios are used to identify the best combination of factor levels allowing to minimize the responses: cutting force and induced damage. As shown in Table 6, the cutting force for this case varies from 20 to 100 N/mm. In Fig. 10 are reported the effects of the four factors on the cutting force, using the means in Fig. 10a and the S/N ratios in Fig. 10b. The results indicate that the fiber orientation (A) and the depth of cut (C) are the most significant factors affecting the force. The rake angle has less contribution on the response and it can be concluded, from these results, that the cutting force have a trend to decrease in a moderate way in passing of a negative rake angle to a positive rake angle. This tendency is also observed in the experimental works of Arola et al. [8] and numerical studies of Lasri et al. [25, 26] and Santiuste et al. [28, 29]. The effect of tool edge radius is insignificant and, therefore, it could be set at the highest level, or at the lowest level, to prolong the tool life depending on the need for the application. According to these results, the optimal combination for a low cutting force is $A_1B_3C_3D_1$ within the tested range. Furthermore, there are no conflicts in determining the optimal solution, using the criteria of the lowest response and highest S/N ratio.

For the induced damage, the computed values varied from 11 to 130 μm as shown in Table 6 and the effects of factors are reported in Fig. 11. The fiber orientation and depth of cut are the main parameters affecting the response followed by the tool rake angle. The tool edge radius is insignificant. This factor could be set at the highest, medium, or lowest level. The best level of the fiber orientation is the lowest of the tested range. Indeed, the damage increases with increasing orientation. These results are in good agreement with the observed trend in different studies which deal with the subsurface damage [22, 24, 26, 28].

For example, for Nayak et al. [24], the simulated damage induced varies within a relatively narrow range for a fiber orientation at 45°. However, for fiber orientations above 45°,

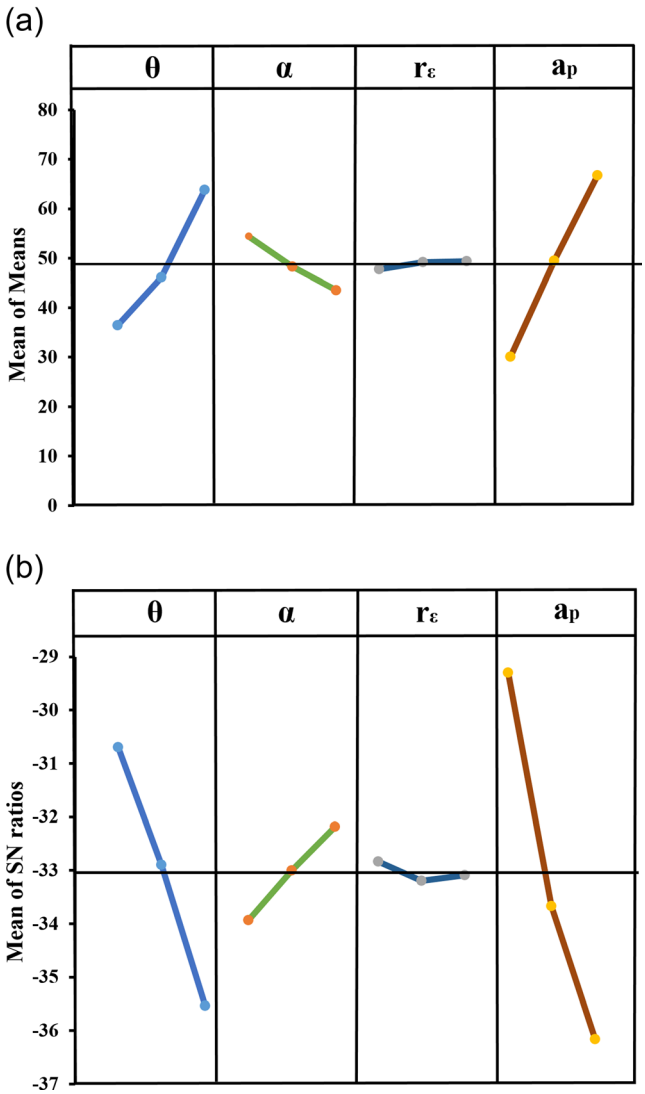

Fig. 10 **a** Fc means and **b** S/N ratio effects for each control factor

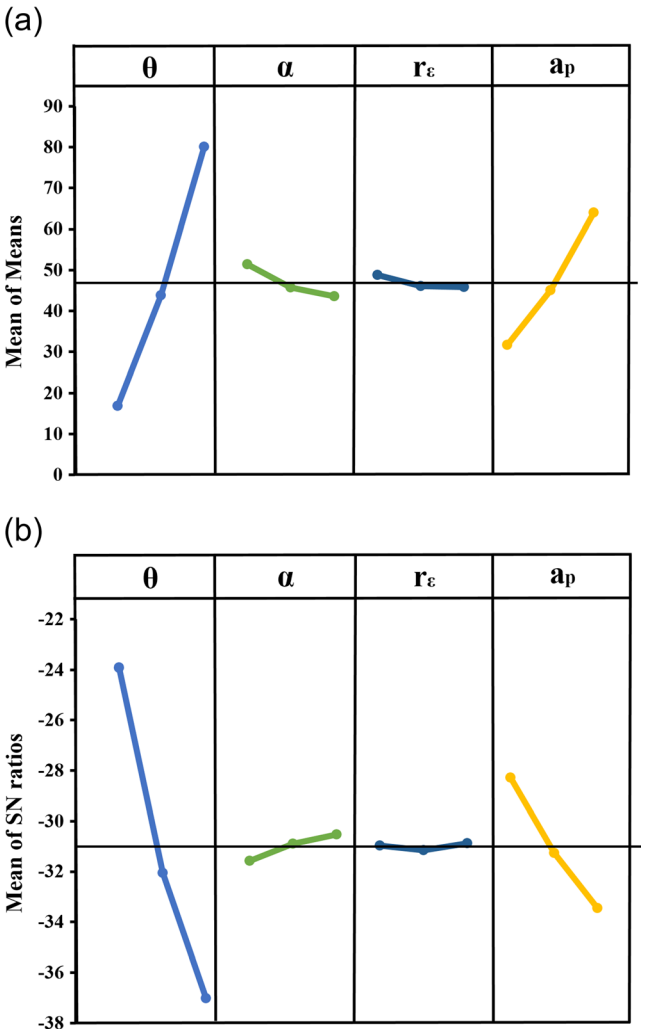

Fig. 11 **a** dm means and **b** S/N ratio effects for each control factor

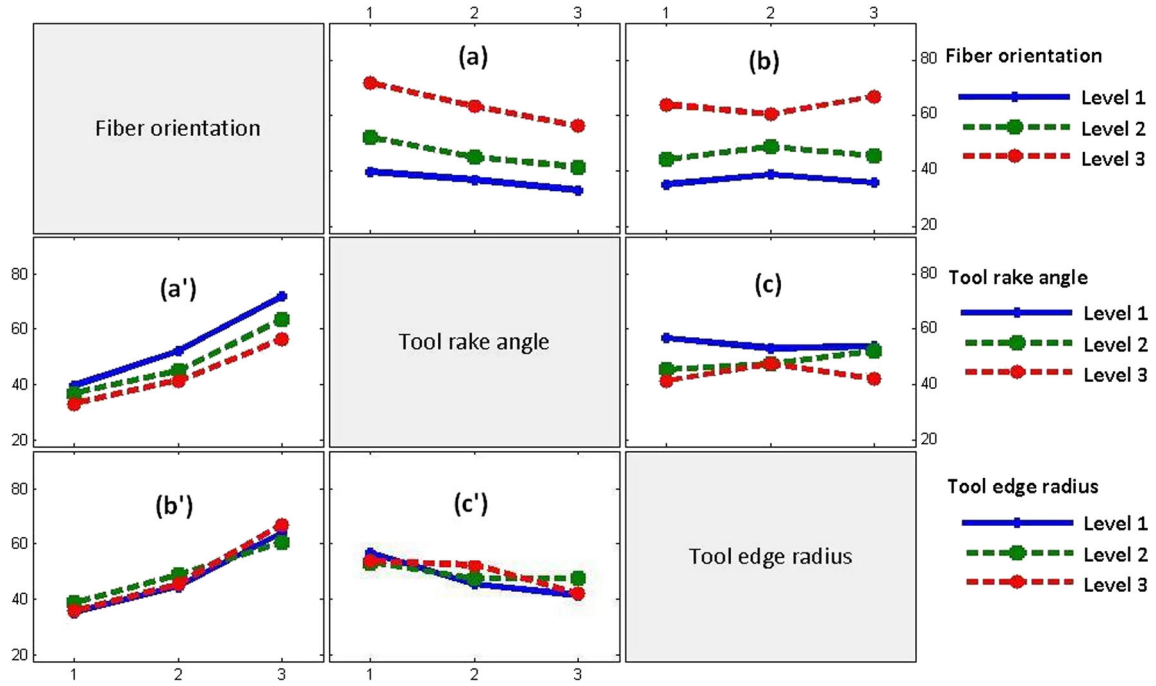

Fig. 12 Interaction plot for cutting force

the variation of the induced damage is more pronounced. This can be verified by the result of Fig. 11 which shows that the difference of damage between fiber orientations 45 and 75° is greater than that between the orientations 45 and 15°.

Besides, the rake angle factor gives the lowest value at third level. According to the effects plot for the induced damage, the optimum combination is $A_1B_3C_3D_1$, which corresponds to the largest value of S/N ratio for all control parameters.

The interaction plots between the parameters fiber orientation (A), tool rake angle (B), and tool edge radius (C) on cutting force, and induced damage are presented in Figs. 12 and 13, respectively. The interaction between the factors is minimal if the lines are parallel for the different levels; otherwise, an interaction exists. For the cutting force, the figures (Fig. 12a, b, a′, and b′) indicated that the interactions between the fiber orientation and both rake angle and tool edge radius

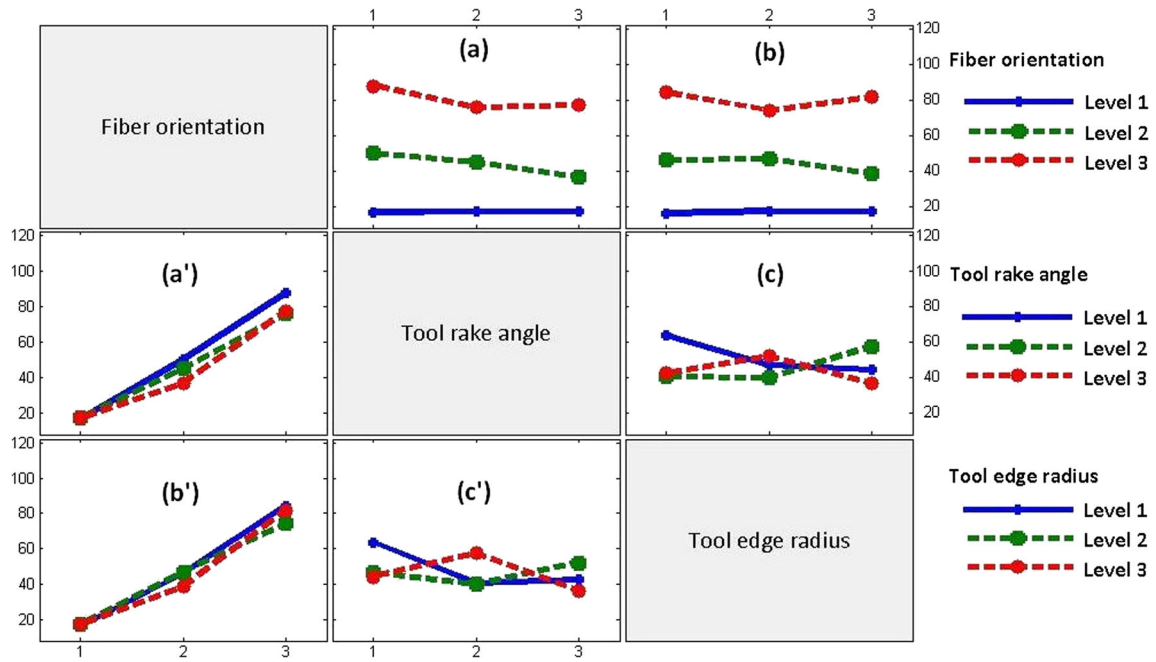

Fig. 13 Interaction plot for induced damage

may be considered low. Referring to the interaction plot of these figures, it was noticed that the cutting force becomes low with the lower value of fiber orientation particularly with the higher tool rake angle. The tool edge radius does not have any significant role on the cutting force. The interaction between tool rake angle and tool edge radius (Fig. 12c and c′) may be considered more significant than the other interactions. It is interpreted from the plots that an increase in tool rake angle results in a decrease of cutting force slightly nonlinear for all values of tool edge radius.

For the induced damage, the interactions (AB and AC) given in Fig. 13a, b, a′, and b′ between fiber orientation and both tool rake angle and tool edge radius are insignificant, and thus a linear model could be used to evaluate the response in the proposed ranges. Furthermore, a significant interaction was found between tool rake angle and tool edge radius and a nonlinear model must be used. From the figures (Fig. 13c′ and c′), it has been noted that high rake angle is preferred in cutting of CFRP composite materials.

5 Conclusion

Machining composites involves a great number of physical parameters. The proposed study provides valuable information to understand the complex interactions between geometrical parameters, cutting conditions, and composite characteristics (fiber orientation, fiber nature, matrix, damage modes, etc.). The main contribution of this work concerns the analysis of the cutting parameters effect and their interactions with cutting force and subsurface damage. To describe the behavior of the CFRP material, an elastoplastic damage model has been adopted to simulate the cutting process. For the optimization procedure, a DoE has been coupled with the numerical simulations in order to study the influence of the cutting parameters on the stability of the machining process. Based on this numerical study, the following conclusions can be drawn:

1. The major factors which control the cutting force and the induced damage are (1) the fiber orientation, (2) the depth of cut, and (3) the tool rake angle. An increase in the fiber orientation and the depth of cut leads to an increase in the cutting force and induced damage levels. The augmentation of the rake angle value implies a decrease of the cutting force and the damage level. It can be said that the tool edge radius almost has no significant effect for the cutting force and damage.
2. It has been noticed that there is significant interaction between tool rake angle and tool edge radius on both responses: cutting forces and induced damage. The interactions between fiber orientation and other parameters (rake angle and tool edge radius) may be neglected.
3. The cutting force and the induced damage in orthogonal cutting of unidirectional CFRP were highly dependent on fiber orientation. Both responses increase linearly with fiber orientation and depth of cut in the studied ranges, [from 15 to 75°] and [from 0.1 to 0.3 mm], respectively. The numerical investigation based on the Taguchi method shows that the lowest cutting force was detected for fiber orientation in the vicinity of 15° and the highest value was observed in the vicinity of 75°.

Also, we intend to expand the application field of the proposed model and to study other benchmark tests of the machining process. Furthermore, optimization algorithms could be combined with the Taguchi method to improve the optimal solution.

As a future work, the model will be extended to a 3D drilling process taking into account the interlaminar delamination phenomenon. Also, the thermomechanical behavior of composites will be considered.

References

1. Liu DF, Tang YJ, Cong WL (2012) A review of mechanical drilling for composite laminates. Compos Struct 94:1265–1279
2. Tsao CC, Hocheng H (2008) Evaluation of thrust force and surface roughness in drilling composite material using Taguchi analysis and neural network. J Mater Proc Technol 203(1–3):342–348
3. Vijayan K, Karthi P, Ramanathan A, Elanghovan M, Senthil Kumar M, Zitoune R, Davim JP (2012) Optimisation of machining parameters at high speed drilling of carbon fiber reinforced plastic (CFRP) laminates. Compos Part B 43(4):1791–1799
4. Koplev A (1980) Cutting on CFRP with single edge tools. In: Proceedings of the Third International Conference on Composite Materials, Paris 2:1597–1605
5. Koplev A, Lystrup A, Vorm T (1983) The cutting process, chips and cutting forces in machining CFRP. Composites 14(4):371–376
6. Wang DH, Ramulu M, Arola D (1995) Orthogonal cutting mechanisms of graphite/epoxy composite part I: unidirectional laminate. Int J Mach Tool Manul 35(12):1623–1638
7. Bhatnagar N, Ramakrishnan N, Naik NK, Komanduri R (1995) On the machining of fiber reinforced plastic (FRP) composite laminates. Int J Mach Tool Manuf 35(5):701–716
8. Arola D, Ramulu M, Wang DH (1996) Chip formation in orthogonal trimming of graphite/epoxy. Compos Part A 27:121–133
9. Ugo EE, Sherif El-Gizawy A, Chukwujekwu Okafor A (2001) An approach for development of damage-free drilling of carbon fiber reinforced thermosets. Int J Mach Tool Manuf 41:1795–1814
10. Palanikumar K (2011) Experimental investigation and optimisation in drilling of GFRP composites. Measurement 44:2138–2148
11. Rajasekaran T, Palanikumar K, Arunachalam S (2013) Investigation on the turning parameters for surface roughness using Taguchi analysis. Procedia Engineering 51:781–790
12. J.S. Pang, M.N.M. Ansari, Omar S. Zaroog, Moaz H. Ali, S.M. Sapuan. Taguchi design optimization of machining parameters on the CNC end milling process of halloysite nanotube with aluminium reinforced epoxy matrix (HNT/Al/Ep) hybrid composite. HBRC Journal 2013

13. Arola D, Ramulu M (1997) Orthogonal cutting of fiber-reinforced composites: a finite element analysis. Int J Mach Tool Manuf 39(5):597–613
14. Ramesh MV, Seetharamu KN, Ganesan N, Sivakumar MS (1998) Analysis of machining of FRPs using FEM. Int J Mach Tools Manuf 38(12):1531–1549
15. Arola D, Sultan MB, Ramulu M (2002) Finite element modeling of edge trimming fiber-reinforced plastics. transaction of ASME J Eng Mater and Technol 124:32–41
16. Lasri L, Nouari M, El-Mansori M (2009) Modelling of chip separation in machining unidirectional FRP composites by stiffness degradation concept. Compos Sci Technol 69:684–692
17. ABAQUS Documentation for version 6.11-2 Dassault systems Simulia, 2011
18. Rao GVG, Mahajan P, Bhatnagar N (2007) Micro-mechanical modeling of machining of FRP composites. Cutting force analysis. Compos Sci Technol 67:579–593
19. Zitoune R, Collombet F, Lachaud F, Piquet R, Pasquet P (2005) Experimental calculation of the cutting conditions representative of the long fiber composite drilling Phase. Compos Sci Techno 65:455–466
20. Wang XM, Zhang LC (2003) An experimental investigation into the orthogonal cutting of unidirectional fibre reinforced plastics. Int J of Mach Tool Manuf 43:1015–1022
21. Jamal YCA. Machining of polymer composites. Springer 2009
22. Bhatnagar N, Nayak D, Singh I, Chouhan H, Mahajan P (2004) Determination of machining-induced damage characteristics of fiber reinforced plastic composite laminates. Mater Manuf Process 19(6): 1009–1023
23. Mahdi M, Zhang L (2001) A finite element model for the orthogonal cutting of fiber reinforced composite materials. J Mater Process Technol 113(1–3):373–377
24. Nayak D, Bhatnagar N, Mahajan P (2005) Machining studies of UD-FRP composites part 2: finite element analysis. Machining Sci Technol 9:503–528
25. Lasri L. Modélisation macromécanique et micromécanique de l'usinage des composites à matrice polymère et fibres longues. PhD thesis; 2009
26. Lasri L, Nouari M, El-Mansori M (2011) Wear resistance and induced cutting damage of aeronautical FRP components obtained by machining. Wear 271(9–10):2542–2548
27. Iliescu D, Gehin D, Iordanoff I, Girot F, Gutiérrez ME (2010) A discrete element method for the simulation of CFRP cutting. Compos Sci Technol 70:73–80
28. Santiuste C, Soldani X, Miguélez HM (2010) Machining FEM model of long fiber composites for aeronautical components. Compos Struct 92:691–698
29. Soldani X, Santiuste C, Muñoz-Sánchez A, Miguélez H (2011) Influence of tool geometry and numerical parameters when modelling orthogonal cutting of LFRP composites. Compos Part A 42:1205–1216
30. Calzada KA, Kapoor SG, DeVor RE, Samuel J, Srivastava AK (2011) Modeling and interpretation of fiber orientation-based failure mechanisms in machining of carbon fiber-reinforced polymer composites. J Manuf Processes 14:141–149
31. Lemaitre J, Chaboche JL. Mechanics of solid materials. Cambridge University Press 1990; Cambridge, UK
32. Crisfield MA. Non-linear finite element analysis of solids and structures. Volume 1: essentials. Wiley 1991
33. Ladeveze P, LeDantec E (1992) Damage modelling of the elementary ply for laminated composites. Compos Sci Technol 43:257–267
34. Allix O, Feissel P, Thévenet P (2003) A delay damage mesomodel of laminates under dynamic loading basic aspects and identification issues. Comput Struct 81:1177–1191
35. Lubineau G, Ladevèze P (2008) Construction of a micromechanics-based intralaminar mesomodel, and illustrations in ABAQUS/Standard. Comput Mater Sci 43(1):137–145
36. Allix O, Deü JF (1997) Delay-damage modelling for fracture prediction of laminated composites under dynamic loading. Eng Trans 45:29–46
37. Ladevèze P, Allix O, Deü JF, Lévêque D (2000) A mesomodel for localisation and damage computation in laminates. Comput Meth Appl Mech Engrg 183:105–122
38. Feld, N. Vers un pont micro-méso de la rupture en compression des composites stratifiés. PhD thesis; pp 115, 2011
39. Schimmerling P, Sisson JC, Zaïdi A (1998) Pratique des plans d′ expériences. Lavoisier, Paris